Spontaneous emission from a two-level atom in a bisphere microcavity

Tetsuyuki Ochiai,[1] Jun-ichi Inoue,[1] and Kazuaki Sakoda[1,2]
[1]*Quantum Dot Research Center, National Institute for Materials Science (NIMS), Tsukuba 305-0044, Japan*
[2]*Graduate School of Pure and Applied Sciences, University of Tsukuba, Tsukuba 305-8577, Japan*
(Received 17 April 2006; published 18 December 2006)

Dynamics of the spontaneous emission from a two-level atom embedded in a bisphere microcavity is analyzed theoretically. A bisphere supports a morphology-dependent resonance having such a high quality factor with local field enhancement that the strong coupling between the atom and the cavity can be realized. By taking full account of the photon degree of freedom, we derive theoretically the coupling constant between the atom and the cavity as well as the radiation damping constants, which are used in the conventional cavity QED approach. In addition, we show that the power spectrum of the spontaneous emission at a local observation point is strongly affected by the photon Green function.

DOI: 10.1103/PhysRevA.74.063818 PACS number(s): 42.50.Pq, 42.50.Ct, 42.55.Sa

I. INTRODUCTION

Recently, various cavities with high quality factor Q have been fabricated in visible and near-infrared frequency ranges [1]. Among them, photonic crystal microcavity is promising, because it offers much smaller modal volume V_m compared to other kinds of high Q cavity [2,3]. Another candidate of high Q with small V_m may be bisphere microcavity. As is well known, an isolated microsphere acts as an open cavity with high Q, because it supports whispering gallery modes with very long lifetimes [4]. These modes are localized near the sphere surface, having rather large V_m. By placing two microspheres in contact, these modes couple more strongly than in a simple bonding/antibonding picture, giving rise to a local field enhancement near the contact point [5]. This may yield small V_m. The bisphere microcavity is versatile in physics, though it has rather simple geometry. It can be regarded as a toy model of coupled cavities in the photonic crystal. Because of its simplicity, various theoretical treatments can be easily adapted to it. In addition, the bisphere microcavity is a photonic molecule, from which fundamental issues in the photonic crystal, e.g., band-formation problem, are extracted [6,7]. Moreover, the bisphere microcavity is an example of a structured reservoir of quantized radiation modes, which may reveal non-Markovian properties [8]. Thus, light-matter interaction, which is described in the framework of quantum electrodynamics, becomes pronounced there.

When we consider microcavity as a stage for cavity quantum electrodynamics (cQED) [9], high Q/V_m is desirable for the Purcell enhancement of the spontaneous emission (SE) of an excited atom embedded in the microcavity [10]. Moreover, high $Q/\sqrt{V_m}$ can lead to the strong coupling between the atom and the cavity, giving rise to the vacuum Rabi splitting of the emission spectrum. In this context, recently, several groups have reported the strong coupling in cQED systems of quantum dots and semiconductor microcavities [11–13]. To predict theoretically various interesting phenomena in the strong-coupling regime, precise evaluation of Q and V_m as well as cQED parameters g, κ, and γ [14] is in order.

Here, we present a theoretical method to evaluate these parameters in a bisphere microcavity coupled to a two-level atom. As for cQED systems of isolated microsphere, microdisk, and microtoroid, there is extensive literature on both theory and experiment [15–25]. However, to the best of our knowledge, only limited works have been reported in the bisphere system [26]. We focus on the simplest cQED effect, namely, a modulated SE from the isolated two-level atom. The key ingredient in the SE dynamics is the local optical density of states (LDOS) [27], which is accessible classically by calculating the dyadic Green tensor of Maxwell's equation [28]. Around the eigenfrequency of a cavity mode, the LDOS can be approximated with the sum of constant and Lorentzian terms as a function of frequency. The coefficients of these two terms are directly related to the cQED parameters, if the transition dipole moment of the two-level atom is given. Since our theoretical approach involves a precise evaluation of the photon Green function, we can extract local optical properties of the system. In particular, it is possible to derive the power spectrum of the SE at a local observation point. The local spectrum is shown to be the product of the conventional SE spectrum of the two-level atom and the term that is relevant to the photon Green function. Therefore, a significant correction from the conventional spectrum may arise in the local spectrum.

This paper is organized as follows. Section II is devoted to the presentation of a theoretical formalism of the SE by using the photon Green function in a general structured reservoir. In Sec. III we present a recipe to determine the cQED parameters. In Sec. IV the vector spherical wave expansion is employed to derive the photon Green function in a cluster of microspheres as an example of a structured reservoir. Numerical results of cavity modes and the SE spectra in a bisphere system are given in Sec. V. Finally, we summarize the results.

II. SPONTANEOUS EMISSION IN A STRUCTURED RESERVOIR

Suppose that an isolated two-level atom is placed in a structured reservoir of quantized radiation modes . The electron in the upper level ($|e\rangle$ with energy E_e) at $t=0$ decays into the lower level ($|g\rangle$ with energy E_g) by emitting one photon in the reservoir. A reservoir photon is specified by state index

α with eigenfrequency ω_α, which is obtained by diagonalizing Maxwell's equation for the spatially dependent dielectric function $\varepsilon(\mathbf{x})$ of the reservoir. In free space, index α corresponds to a pair of polarization and wave-number vectors. The decay process is described by the wave function,

$$|\psi(t)\rangle = b(t)e^{-iE_e t/\hbar}|e,0\rangle + \sum_\alpha c_\alpha(t)e^{-i(\omega_\alpha + E_g/\hbar)t}|g,\alpha\rangle. \quad (1)$$

The time evolution of $|\psi(t)\rangle$ is determined by the following interaction Hamiltonian [29]:

$$H_{\text{int}} = \sum_\alpha (g_\alpha \hat{c}_\alpha \hat{a}_e^\dagger \hat{a}_g + \text{H.c.}), \quad (2)$$

$$g_\alpha = i\sqrt{\frac{\hbar\Omega^2}{2\varepsilon_0\omega_\alpha V}}\mathbf{d}\cdot\mathbf{E}_\alpha(\mathbf{x}_d), \quad (3)$$

$$\Omega = (E_e - E_g)/\hbar. \quad (4)$$

Here, $\hat{c}_\alpha$ is the annihilation operator of reservoir state α, $\hat{a}_e^\dagger$ is the creation operator of the electron in the upper level, $\hat{a}_g$ is the annihilation operator of the electron in the lower level, and H.c. represents the Hermitian conjugate. The coupling between the two-level atom and the reservoir state is given by the inner product of the dipole moment $\mathbf{d}$ of the two-level atom and the electric-field eigenfunction $\mathbf{E}_\alpha(\mathbf{x}_d)$ of the reservoir state, $\mathbf{x}_d$ being the position of the two-level atom. The eigenfunction is normalized as

$$V = \int d^3x\varepsilon(\mathbf{x})|\mathbf{E}_\alpha(\mathbf{x})|^2, \quad (5)$$

where V is the normalization volume.

By solving the Schrödinger equation, amplitude $b(t)$ of the excited state is shown to satisfy

$$\frac{db(t)}{dt} = -\int_0^t dt' K(t-t')b(t'), \quad (6)$$

$$K(t-t') = \int d\omega \tilde{K}(\omega)e^{-i(\omega-\Omega)(t-t')}, \quad (7)$$

$$\tilde{K}(\omega) = \frac{\Omega^2|\mathbf{d}|^2}{6\varepsilon_0\hbar\omega}\rho(\mathbf{x}_d;\omega). \quad (8)$$

Here, $\rho(\mathbf{x};\omega)$ is the LDOS of the reservoir, and is defined by

$$\rho(\mathbf{x};\omega) = \frac{1}{V}\sum_\alpha |\mathbf{E}_\alpha(\mathbf{x})|^2\delta(\omega-\omega_\alpha). \quad (9)$$

Let us focus on the power spectrum at a local observation point given by $\mathbf{x}$. The definition of the spectrum is [30]

$$I(\mathbf{x};\omega) = \int_0^\infty dt_1 dt_2 e^{-i\omega(t_1-t_2)}\langle \mathbf{E}^-(\mathbf{x},t_1)\cdot\mathbf{E}^+(\mathbf{x},t_2)\rangle, \quad (10)$$

where the Heisenberg representation is used for the electric-field operator $\mathbf{E}$. The superscript of $\mathbf{E}$ stands for either positive (+) or negative (−) frequency part as usual. This spectrum becomes

$$I(\mathbf{x};\omega) = f(\mathbf{x};\omega)S(\omega), \quad (11)$$

$$f(\mathbf{x};\omega) = \frac{1}{3}\left(\frac{\pi\Omega|\mathbf{d}|}{\varepsilon_0}\right)^2\sum_{i,j}|\rho_{ij}(\mathbf{x},\mathbf{x}_0;\omega)|^2, \quad (12)$$

$$S(\omega) = \int_0^\infty dt_1 dt_2 e^{-i\omega(t_1-t_2)}\langle\sigma^+(t_1)\sigma^-(t_2)\rangle \quad (13)$$

$$= \left|\int_0^\infty dt e^{i(\omega-\Omega)t}b(t)\right|^2, \quad (14)$$

$$\rho_{ij}(\mathbf{x},\mathbf{x}';\omega) = \frac{1}{V}\sum_\alpha (\mathbf{E}_\alpha(\mathbf{x}))_i(\mathbf{E}_\alpha(\mathbf{x}'))_j^*\delta(\omega-\omega_\alpha). \quad (15)$$

Here, $\sigma^+ = \hat{a}_e^\dagger\hat{a}_g$, $\sigma^- = \hat{a}_g^\dagger\hat{a}_e$, and $S(\omega)$ is equal to the conventional definition of the emission spectrum from a two-level atom [14].

In the above argument there are two important quantities of the reservoir, namely, the LDOS $\rho(\mathbf{x};\omega)$ and its nonlocal counterpart $\rho_{ij}(\mathbf{x},\mathbf{x}';\omega)$. Both of them are directly related to the photon Green function, or in other words, the dyadic Green tensor of Maxwell's equation, whose definition is given by

$$\nabla\times\nabla\times\overleftrightarrow{G}(\mathbf{x},\mathbf{x}';\omega) - \frac{\omega^2}{c^2}\varepsilon(\mathbf{x})\overleftrightarrow{G}(\mathbf{x},\mathbf{x}';\omega) = \overleftrightarrow{1}\delta(\mathbf{x}-\mathbf{x}'). \quad (16)$$

Here, the arrow denotes the omission of the tensor index [$(\overleftrightarrow{G})_{ij} = G_{ij}$ and $(\overleftrightarrow{1})_{ij} = \delta_{ij}$ is the Kronecker delta]. From this definition, the following relations are obtained:

$$\rho(\mathbf{x};\omega) = \frac{2\omega}{\pi c^2}\,\text{Im Tr}\,\overleftrightarrow{G}(\mathbf{x},\mathbf{x};\omega), \quad (17)$$

$$\rho_{ij}(\mathbf{x},\mathbf{x}';\omega) = \frac{\omega}{i\pi c^2}[G_{ij}(\mathbf{x},\mathbf{x}';\omega) - G_{ji}^*(\mathbf{x}',\mathbf{x};\omega)]. \quad (18)$$

The dyadic Green tensor is accessible classically, by solving the dipole radiation problem in the reservoir. This is indeed possible as indicated in Sec. IV.

In free space, the difference between the power spectrum $I(\mathbf{x};\omega)$, which can be measured experimentally, and the emission spectrum $S(\omega)$ is not remarkable. This is because the term $f(\mathbf{x};\omega)$ has a rather simple dependence on ω in free space, and thus has no pronounced effect. However, this is not the case in a structured reservoir owing to a nontrivial ω dependence of $f(\mathbf{x};\omega)$. Therefore, we have to be careful about the difference.

III. CAVITY QED PARAMETERS

In the previous section we derived various formulas of the SE in a general structured reservoir by using the photon Green function. The formulas are obtained by taking full account of the photon degree of freedom in a reservoir. If the

reservoir acts as a cavity, the SE is affected by cQED effects. In the conventional approach to the SE in a cavity, a two-level atom is assumed to interact with a single cavity mode with eigenfrequency ω_c via the Jaynes-Cummings Hamiltonian with coupling g. Then, the radiation damping of the two-level atom is introduced phenomenologically with two parameters, namely, the SE rate γ into free space and the photon decay rate κ from the cavity [14]. By solving the master equation of the density matrix, we can obtain analytically various quantities such as the emission spectrum of the two-level atom.

In contrast, our approach given in Sec. II starts with the two-level atom interacting with an infinite number of reservoir modes via the minimal coupling. We do not distinguish a cavity mode from other reservoir modes. The radiation damping of the two-level atom is explained with the spectral function, namely, the LDOS of the reservoir, such as in the Caldeira-Leggett model for quantum dissipation [31]. Although this approach has been employed by several authors [29,32–34], the relation between this approach and the conventional one is not yet clarified. Therefore, it is desirable to relate them, in particular, to identify the cQED parameters g, κ, and γ of the conventional one, which play a crucial role in the SE dynamics.

Suppose that the LDOS is approximated with the sum of constant and Lorentzian terms as

$$\omega\frac{\rho(\mathbf{x};\omega)}{\rho_0(\omega)} = \omega_c\left(\xi_0 + \frac{\xi_1\omega_c^2}{(\omega-\omega_c)^2 + \left(\frac{\omega_c}{2Q}\right)^2}\right), \tag{19}$$

where $\rho_0(\omega)=\omega^2/(\pi^2c^3)$ is the (local) optical density of states in vacuum. The above spectral profile corresponds to an open cavity with eigenfrequency ω_c and quality factor Q. The constant term stands for the background LDOS, which explains the contribution of the reservoir eigenmodes independent of the relevant cavity mode. The Lorentzian term stands for the cavity mode with loss. The dimensionless parameters ξ_0 and ξ_1 represent the intensities of these two terms, and have $\mathbf{x}$ dependence implicitly. Using the above approximation, the Fourier transform of the memory kernel given in Eq. (8) is expressed as

$$\tilde{K}(\omega) = \frac{1}{\pi}\left(\frac{\gamma}{2} + \frac{g^2\kappa}{(\omega-\omega_c)^2+\kappa^2}\right), \tag{20}$$

$$g = \sqrt{\frac{\Omega^2\omega_c^2|\mathbf{d}|^2Q\xi_1}{3\pi\varepsilon_0c^3\hbar}}, \tag{21}$$

$$\kappa = \frac{\omega_c}{2Q}, \tag{22}$$

$$\gamma = \frac{\Omega^2\omega_c|\mathbf{d}|^2Q\xi_0}{3\pi\varepsilon_0c^3\hbar}. \tag{23}$$

In this case $b(t)$ can be solved analytically by using the Laplace transformation. The result is given by

$$b(t) = \frac{s_+ + \kappa + i(\omega_c-\Omega)}{s_+ - s_-}e^{ts_+} - \frac{s_- + \kappa + i(\omega_c-\Omega)}{s_+ - s_-}e^{ts_-}, \tag{24}$$

$$s_\pm = \frac{1}{2}\left[-\left(\kappa + i(\omega_c-\Omega) + \frac{\gamma}{2}\right) \pm \sqrt{\left(\kappa + i(\omega_c-\Omega) - \frac{\gamma}{2}\right)^2 - 4g^2}\right]. \tag{25}$$

When the argument of the square root in $s_\pm$ is negative at zero detuning ($\omega_c=\Omega$), the system is in the strong-coupling regime. Otherwise, it is in the weak-coupling regime. This criterion is the same as in the conventional approach using the master equation [14].

Using the expression of $b(t)$, we can obtain analytically the emission spectrum of the two-level atom,

$$S(\omega) = \left|\frac{1}{s_+ - s_-}\left(\frac{s_+ + \kappa + i(\omega_c-\Omega)}{s_+ + i(\omega-\Omega)} - \frac{s_- + \kappa + i(\omega_c-\Omega)}{s_- + i(\omega-\Omega)}\right)\right|^2, \tag{26}$$

which is again equal to that given in Refs. [14,35] at zero detuning. Therefore, our parameters g, κ, and γ are exactly equal to those used in the conventional approach.

For further correspondence to the conventional cQED concept, we can introduce the modal volume V_m of the cavity as follows. If $\mathbf{x}$ is at the maximum spatial point $\mathbf{x}_{\max}$ of $\rho(\mathbf{x};\omega_c)$, ξ_1 is related to the mode volume of the cavity as

$$\xi_1 \approx \frac{\pi c^3}{2\varepsilon(\mathbf{x}_{\max})\omega_c^3QV_m}, \tag{27}$$

$$V = \varepsilon(\mathbf{x}_{\max})|\mathbf{E}_c(\mathbf{x}_{\max})|^2V_m. \tag{28}$$

However, we should note that the modal volume is an associate quantity of LDOS, and that it can be defined rigorously only if the cavity mode is square integrable (or in other words, Q is infinite). Of primary importance in the SE is not the modal volume, but the LDOS.

It is interesting to ask how ξ_0 and ξ_1 are related to geometrical parameters of a conventional Fabry-Pérot cavity composed of two parallel mirrors. In the geometrical optics limit, it was shown that these parameters are related to the solid angle covered by the mirrors, the distance between the mirrors, and the reflectance of the mirrors [36]. However, if the relevant wavelength is comparable with the size of the cavity, the relation becomes nontrivial. Nevertheless, it is possible to derive ξ_0 and ξ_1 numerically by calculating the LDOS in the cavity via, for instance, the finite-difference time-domain method [37].

Finally, we should comment on a way to improve the approximation used in Eq. (19). At least locally around a sharp peak of the LDOS, it is reasonable to approximate the LDOS as the sum of a constant term and a Lorentzian term. To improve the approximation, we can include effects of other nearby peaks by introducing the corresponding Lorentzian terms in the LDOS. The constant term in LDOS can also be written as a special limit of the Lorentzian term. There-

fore, an improved expression of the LDOS is given by a sum of Lorentzian terms having different ω_c, ξ_1, and Q. Even in this case, we can derive the semi-analytic expression of the emission spectrum $S(\omega)$ of the two-level atom. Suppose that the LDOS is given by

$$\omega\frac{\rho(\mathbf{x};\omega)}{\rho_0(\omega)} = \sum_j \frac{\xi_{1j}\omega_{cj}^3}{(\omega-\omega_{cj})^2 + \left(\frac{\omega_{cj}}{2Q_j}\right)^2}. \tag{29}$$

By introducing the corresponding parameters g_j and κ_j in accordance with Eqs. (21) and (22), the resultant expressions of $b(t)$ and $S(\omega)$ become

$$b(t) = \sum_j e^{ts_j}\frac{P_n(s_j)}{P'_{n+1}(s_j)}, \tag{30}$$

$$S(\omega) = \left|\sum_j \frac{1}{s_j + i(\omega-\Omega)}\frac{P_n(s_j)}{P'_{n+1}(s_j)}\right|^2, \tag{31}$$

where $P_{n+1}(s)$ and $P_n(s)$ are the denominator and numerator, respectively, of the rational expression of

$$\frac{1}{s + \sum_j \frac{g_j^2}{s+\kappa_j + i(\omega_{cj}-\Omega)}}\left(= \int_0^\infty dt e^{-st}b(t)\right). \tag{32}$$

Here, n is the number of the Lorentzian peaks and s_i is a root of the $n+1$th-order polynomial $P_{n+1}(s)$. The spectral shape of $S(\omega)$ depends crucially on ω_c, ξ_1, and Q of the Lorentzian peaks, and the clear criterion of the weak or strong coupling becomes lost. We will discuss the effects of the improvement in Sec. V.

IV. VECTOR SPHERICAL WAVE EXPANSION OF THE PHOTON GREEN FUNCTION

So far, we have argued properties of the SE in a general structured reservoir. From now on, we focus on a cluster of nonoverlapping microspheres as a reservoir because sophisticated analytical approach, namely, vector spherical wave expansion, can be applied for the photon Green function. This yields a precise evaluation of the power spectrum of the SE at a local observation point.

As is well known, an isolated microsphere can support whispering gallery modes with high Q at particular frequencies. They are classified according to angular momentum (l,m) as well as polarization. It should be pointed out here that there is a $(2l+1)$-fold degeneracy with respect to m. This yields a spherically symmetric profile of the LDOS of the isolated sphere. The whispering gallery mode is nothing but the Mie resonance with high angular momentum [38]. This resonance is an optical analogue of a metastable state trapped by a confining potential in quantum mechanics. [The dielectric function $\varepsilon(\mathbf{x})$ acts as a confining potential of the photon if $\varepsilon(\mathbf{x})>1$]. Owing to the strong centrifugal force due to the high angular momentum, the mode is localized close to the surface of the sphere. A cluster of microspheres also can support similar resonant eigenmodes, which are known as morphology-dependent resonances. The physical origin of the resonances is the coupling among the whispering gallery modes of each sphere. On the contrary to the isolated sphere, in a cluster of microspheres, it is possible to attain hot spots in the LDOS as shown later.

As was mentioned in Sec. II, the photon Green function is obtained by solving the dipole radiation problem. To solve the problem in a cluster of spheres, we employ the multiple-scattering method on the basis of vector spherical waves. A theoretical framework for this problem in a bisphere system was developed in the 1980's in connection to the surface enhanced Raman scattering, where an adsorbed molecule on a metallic particle plays the role of the point oscillating dipole [39]. Here, we extend the framework to deal with an arbitrary number of spheres and with a dipole placed inside a sphere.

The cluster consists of nonoverlapping spheres with dielectric function ε_n and radius r_n $(n=1,2,\ldots,N)$ embedded in a homogeneous medium of dielectric constant ε_b. The center of the nth sphere is denoted by $\mathbf{x}_n$. The point oscillating dipole of harmonic time dependence $e^{-i\omega t}$ is placed at $\mathbf{x}=\mathbf{x}_d$ with dipole polarization vector $\mathbf{d}$. By using the dyadic Green tensor, the electric field induced by the dipole can be written as

$$\mathbf{E}(\mathbf{x}) = \mu_0\omega^2\overleftrightarrow{G}(\mathbf{x},\mathbf{x}_d;\omega)\mathbf{d}. \tag{33}$$

Therefore, the ith Cartesian component of the electric field gives the (i,j)th component of the dyadic Green tensor, if $\mathbf{d}$ is proportional to the unit vector in the x_j direction.

First, let us assume that the dipole is placed outside the spheres. The electric field of the dipole is expanded as

$$\mathbf{E}^0(\mathbf{x}) = \sum_{L,L',\beta} j_l(q_b|\mathbf{R}_n|)Y_L(\hat{\mathbf{R}}_n)[\mathbf{P}^\beta]_{L,L'}\alpha^{\beta,0}_{L',n}, \tag{34}$$

$$\alpha^{\beta,0}_{L,n} = \frac{i\mu_0\omega^2 q_b}{l(l+1)}\sum_{L'}\mathbf{d}\cdot[(\mathbf{P}^\beta)^\dagger]_{L,L'}h_{l'}(q_b|\mathbf{R}_{dn}|)Y^*_{L'}(\hat{\mathbf{R}}_{dn}), \tag{35}$$

$$\mathbf{R}_n = \mathbf{x}-\mathbf{x}_n, \quad \mathbf{R}_{dn} = \mathbf{x}_d - \mathbf{x}_n, \tag{36}$$

if $|\mathbf{R}_n|<|\mathbf{R}_{dn}|$. Here $L=(l,m)$ is the angular momentum, $\beta(=M,N)$ is the two transverse degree of vector spherical wave, j_l is the spherical Bessel function, h_l is the spherical Hankel function of the first kind, Y_L is the spherical harmonics, and $\mathbf{P}^\beta$ is the expansion coefficient of the vector spherical wave into the scalar spherical wave [40]. We also note that $q_b=\sqrt{\varepsilon_b}\omega/c$ is the wave number in the background medium and that $\hat{\mathbf{R}}$ stands for the unit vector parallel to $\mathbf{R}$.

Taking this dipole radiation field as an incident wave, the induced field is generated after through the multiple scattering among the spheres. The induced field outside the spheres is shown to become

$$\mathbf{E}^{\text{out}}(\mathbf{x}) = \sum_n \mathbf{E}^{\text{out}}_n(\mathbf{x}), \tag{37}$$

$$\mathbf{E}_n^{\text{out}}(\mathbf{x}) = \sum_{L,L',\beta} h_l(q_b|\mathbf{R}_n|)Y_L(\hat{\mathbf{R}}_n)[\mathbf{P}^\beta]_{L,L'}\alpha_{L',n}^{\beta,\text{out}}, \quad (38)$$

where $\alpha_{L,n}^{\beta,\text{out}}$ is determined by the following equation [5,41]:

$$\alpha_{L,n}^{\beta,\text{out}} = t_{l,n}^{\beta}\left(\alpha_{L,n}^{\beta,\text{inc}} + \sum_{L',\beta'}\sum_{n'\neq n} H_{(L,n),(L',n')}^{\beta,\beta'}\alpha_{L',n'}^{\beta',\text{out}}\right), \quad (39)$$

$$H_{(L,n),(L',n')}^{\beta,\beta'} = \frac{1}{l(l+1)}\sum_i [(P_i^\beta)^\dagger G_{n,n'}P_i^{\beta'}]_{L,L'}, \quad (40)$$

$$[G_{n,n'}]_{L,L'} = 4\pi\sum_{L''} i^{-l+l'+l''}h_{l''}(q_b|\mathbf{R}_{nn'}|)Y_{L''}(\hat{\mathbf{R}}_{nn'})\langle L'|L''|L\rangle, \quad (41)$$

$$\alpha_{L,n}^{\beta,\text{inc}} = \alpha_{L,n}^{\beta,0}. \quad (42)$$

Here, $\langle L'|L''|L\rangle$ is the Clebsch-Gordan coefficient, and the prefactor $t_{l,n}^{\beta}$ in the right-hand side of Eq. (39) is the so-called t matrix of the nth sphere. Equation (39) can be solved numerically by truncating the angular momentum up to $l=l_{\max}$. Inside the nth sphere the induced field becomes

$$\mathbf{E}_n^{\text{in}}(\mathbf{x}) = \sum_{L,L',\beta} j_l(q_n|\mathbf{R}_n|)Y_L(\hat{\mathbf{R}}_n)[\mathbf{P}^\beta]_{L,L'}\alpha_{L',n}^{\beta,\text{in}}, \quad (43)$$

$$\alpha_{L,n}^{\beta,\text{in}} = s_{l,n}^{\beta,++}(s_{l,n}^{\beta,-+})^{-1}\alpha_{L,n}^{\beta,\text{out}}, \quad (44)$$

where $q_n=\sqrt{\varepsilon_n}\omega/c$ is the wave number inside the nth sphere and $s_{l,n}^{\beta,\pm\pm}$ is the interface S matrix, which is given by

$$\begin{pmatrix} s_{l,n}^{M,++} & s_{l,n}^{M,+-} \\ s_{l,n}^{M,-+} & s_{l,n}^{M,--} \end{pmatrix} = -\frac{1}{d_l^<}\begin{pmatrix} i/\rho_b & d_l^\geqslant \\ d_l^> & i/\rho_a \end{pmatrix}, \quad (45)$$

$$\begin{pmatrix} s_{l,n}^{N,++} & s_{l,n}^{N,+-} \\ s_{l,n}^{N,-+} & s_{l,n}^{N,--} \end{pmatrix} = -\frac{1}{w_l^<}\begin{pmatrix} i/\rho_b & w_l^\geqslant \\ w_l^> & i/\rho_a \end{pmatrix}, \quad (46)$$

$$d_l^< = \rho_a j_l'(\rho_a)h_l(\rho_b) - \rho_b h_l'(\rho_b)j_l(\rho_a), \quad (47)$$

$$d_l^> = \rho_a j_l'(\rho_a)j_l(\rho_b) - \rho_b j_l'(\rho_b)j_l(\rho_a), \quad (48)$$

$$d_l^\geqslant = \rho_a h_l'(\rho_a)h_l(\rho_b) - \rho_b h_l'(\rho_b)h_l(\rho_a), \quad (49)$$

$$w_l^< = \frac{\rho_b}{\rho_a}(\rho_a j_l(\rho_a))'h_l(\rho_b) - \frac{\rho_a}{\rho_b}(\rho_b h_l(\rho_b))'j_l(\rho_a), \quad (50)$$

$$w_l^> = \frac{\rho_b}{\rho_a}(\rho_a j_l(\rho_a))'j_l(\rho_b) - \frac{\rho_a}{\rho_b}(\rho_b j_l(\rho_b))'j_l(\rho_a), \quad (51)$$

$$w_l^\geqslant = \frac{\rho_b}{\rho_a}(\rho_a h_l(\rho_a))'h_l(\rho_b) - \frac{\rho_a}{\rho_b}(\rho_b h_l(\rho_b))'h_l(\rho_a), \quad (52)$$

for the nth sphere. Here, $\varepsilon_a=\varepsilon_n$, $\rho_a=q_n r_n$, and $\rho_b=q_b r_n$. We should note that $t_{l,n}^{\beta}=s_{l,n}^{\beta,-+}$. Thus, the total electric field both inside and outside the spheres is given by

$$\mathbf{E}(\mathbf{x}) = \begin{cases} \mathbf{E}_n^{\text{in}}(\mathbf{x}) & \text{for } |\mathbf{R}_n| < r_n, \\ \mathbf{E}^0(\mathbf{x}) + \mathbf{E}^{\text{out}}(\mathbf{x}) & \text{otherwise.} \end{cases} \quad (53)$$

On the other hand, if the dipole is placed inside the nth sphere in the cluster, the dipole radiation field inside the sphere is expanded as

$$\mathbf{E}^0(\mathbf{x}) = \sum_{L,L',\beta} h_l(q_n|\mathbf{R}_n|)Y_L(\hat{\mathbf{R}}_n)[\mathbf{P}^\beta]_{L,L'}\alpha_{L',n}^{\beta,0}, \quad (54)$$

$$\alpha_{L,n}^{\beta,0} = \frac{i\mu_0\omega^2 q_n}{l(l+1)}\sum_{L'}\mathbf{d}\cdot[(\mathbf{P}^\beta)^\dagger]_{L,L'}j_{l'}(q_n|\mathbf{R}_{dn}|)Y_{L'}^*(\hat{\mathbf{R}}_{dn}), \quad (55)$$

provided $|\mathbf{R}_n|>|\mathbf{R}_{dn}|$. The induced field outside the spheres satisfies the same multiple-scattering equation [Eq. (39)] except that

$$\alpha_{L,k}^{\beta,\text{inc}} = \delta_{k,n}(s_{l,n}^{\beta,-+})^{-1}s_{l,n}^{\beta,--}\alpha_{L,n}^{\beta,0}, \quad (56)$$

which takes account of the scattering by the sphere surface. The multipole coefficient of the induced field inside the kth sphere is given by

$$\alpha_{L,k}^{\beta,\text{in}} = s_{l,k}^{\beta,++}(s_{l,k}^{\beta,-+})^{-1}\alpha_{L,k}^{\beta,\text{out}} + \delta_{k,n}[s_{l,n}^{\beta,+-} - s_{l,n}^{\beta,++}(s_{l,n}^{\beta,-+})^{-1}s_{l,n}^{\beta,--}]\alpha_{L,n}^{\beta,0}. \quad (57)$$

Thus, the total electric field both inside and outside the spheres becomes

$$\mathbf{E}(\mathbf{x}) = \begin{cases} \mathbf{E}^0(\mathbf{x}) + \mathbf{E}_n^{\text{in}}(\mathbf{x}) & \text{for } |\mathbf{R}_n| < r_n, \\ \mathbf{E}_k^{\text{in}}(\mathbf{x}) & \text{for } |\mathbf{R}_k| < r_k \ (k\neq n), \\ \mathbf{E}^{\text{out}}(\mathbf{x}) & \text{otherwise.} \end{cases} \quad (58)$$

Since the electric field induced by the dipole is expressed as Eqs. (53) and (58), the photon Green function $\vec{G}(\mathbf{x},\mathbf{x}_d;\omega)$ is obtained in the entire region of $\mathbf{x}$ and $\mathbf{x}_d$ through Eq. (33). The LDOS is also obtained by taking $\mathbf{x}=\mathbf{x}_d$ of $\vec{G}(\mathbf{x},\mathbf{x}_d;\omega)$ in accordance with Eq. (17).

V. NUMERICAL RESULTS AND DISCUSSIONS

From now on, we concentrate on a bisphere in contact as a model system of a structured reservoir. We further assume that a single two-level atom is loaded into one of two identical spheres ($N=2$, $\varepsilon_1=\varepsilon_2=\varepsilon_a$, $r_1=r_2=a/2$) and that the atom is initially excited. This atom eventually decays into the ground state by emitting photon. Since the two-level atom is a theoretical model of the quantum dot exciton, the bisphere is assumed to be made of a semiconductor such as GaAs, which is usually taken as a host of the quantum dot. In the bisphere system morphology-dependent resonances occur yielding a variety of cavity modes. If the two spheres are well separated, the cavity modes are basically the bonding and antibonding of the whispering gallery modes of each sphere. However, in the case of bisphere in contact, the modes are not simply attributed to the whispering gallery modes, and can exhibit the local field enhancement around the contact point. To take full account of these features, we perform a numerical calculation of the photon Green function and the SE spectra given in the previous sections. A good convergence is obtained with $l_{\max}=25$ in the frequency range of interest.

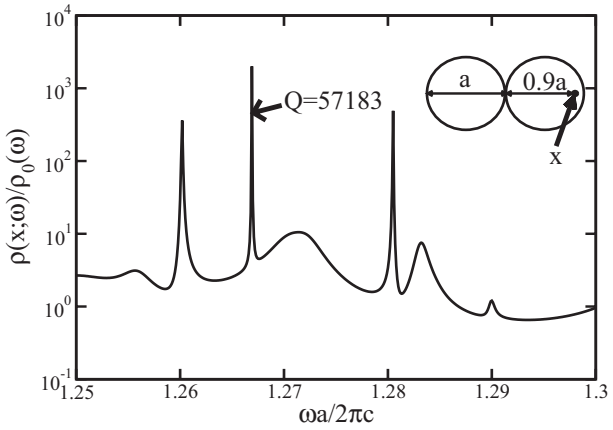

FIG. 1. The normalized LDOS $\rho(\mathbf{x};\omega)/\rho_0(\omega)$ is plotted as a function of frequency at the marked point (shown in the inset) of a bisphere in contact. The dielectric constant and radius of the bisphere were taken to be $\varepsilon_a=12$ and $r=0.5a$, respectively. The background medium is air ($\varepsilon_b=1$).

Figure 1 shows the normalized LDOS at $\mathbf{x}=(0.90a,0,0)$ [This point is a hot spot of the LDOS at a certain frequency (see Fig. 2).] Here, the centers of the two spheres are at $\mathbf{x}_1=(a/2,0,0)$ and $\mathbf{x}_2=(-a/2,0,0)$, and the dielectric constants were taken to be $\varepsilon_a=12$ and $\varepsilon_b=1$. As is seen in Fig. 1, the LDOS exhibits a sequence of peaks, each of which corresponds to a cavity mode in the bisphere. In the frequency interval of Fig. 1, the highest Q $(=0.572\times10^5)$ is obtained at $\omega a/2\pi c=1.2669$. In the whole frequency range below $\omega a/2\pi c=1.5$, the highest Q $(=0.287\times10^6)$ is found at $\omega a/2\pi c=1.3700$. As in an isolated microsphere, the quality factor of a cavity mode generally increases with increasing frequency, so that higher Q can be obtained in $\omega a/2\pi c \geqslant 1.5$. Though several peaks are overlapped, it is reasonable to introduce the approximation given in Eq. (19) around the peak at $\omega_c a/2\pi c=1.2669$. By a numerical fitting, we obtained $\xi_0=0.182$ and $\xi_1=0.153\times10^{-6}$.

The spatial profile of the LDOS at this frequency is shown in Fig. 2. One can observe four hot spots at $(x,y,z)=(\pm0.90a,0,0)$ and $(\pm0.12a,0,0)$, where LDOS becomes 2000 times larger than that in the vacuum. Here, we should point out that the LDOS is invariant under the rotation with respect to the x axis. Since the hot spots appear along this axis, they are of pointlike enhancement. In other words, the pointlike enhancement of the LDOS, if any, has to appear along the axis. Most likely, this hot spot appears near the surface of the bisphere, because the relevant cavity mode is basically a mixture of the whispering gallery modes of each sphere, having large field intensity near the sphere surface. As is obvious in Fig. 2, this is indeed the case in our spatial profile of the LDOS. The hot spots appear at the intersection points between the twin rings of large LDOS in Fig. 2 and the symmetry axis. That is why the four hot spots appear in the bisphere. We confirmed that the four hot spots also appear at the frequencies of the other sharp peaks of the LDOS in Fig. 1. We also note that the vector spherical wave expansion of the LDOS at $\omega a/2\pi c=1.2669$ is mostly governed by the multi-pole component of $\beta=N$ and $l=9$ [see Eqs. (43) and (57)]. As we will see, there is indeed the whispering gallery mode with this component whose eigenfrequency is very close to the cavity eigenfrequency concerned.

The spatial profile of the LDOS provides a striking contrast to that in an isolated sphere, where the pointlike enhancement of the LDOS is completely absent owing to the perfect rotational symmetry of the system. This enhancement is caused by the cavity mode at the same frequency. The cavity modal volume is estimated as $V_m=2.5(\lambda/n)^3$, where λ is the wavelength in vacuum at the cavity eigenfrequency and $n=\sqrt{\varepsilon_a}$. This value of the modal volume is, however, not so small compared with that in the photonic crystal cavity. A typical modal volume is $V_m=0.71(\lambda/n)^3$ for the $L3$ cavity in the triangular photonic crystal slab [2].

Whereas we are interested in the bisphere cavity from various viewpoints, it is instructive to compare the bisphere cavity with the isolated sphere cavity in detail. In the latter case, the rotational symmetry of the system prohibits the mixing of angular momentum, giving rise to ultrahigh Q. Actually, with the same radius ($r=0.5a$) and dielectric constant ($\varepsilon=12$), the LDOS spectrum of the isolated sphere exhibits two sharp peaks in $1.25\leqslant\omega a/2\pi c\leqslant1.30$. They are due to the whispering gallery modes of $\beta=N$, $l=9$, and $\omega a/2\pi c=1.2656$, and of $\beta=M$, $l=10$, and $\omega a/2\pi c=1.2725$. The peak heights (and widths) of the normalized LDOS $\rho(\mathbf{x};\omega)/\rho_0(\omega)$ at distance $0.4a$ from the center of the sphere are evaluated as $3.2\times10^5(Q=5.7\times10^6)$ and $1.3\times10^6(Q=2.1\times10^7)$ for the former and latter peaks, respectively. Therefore, the isolated microsphere cavity has much larger LDOS and higher Q than the bisphere cavity has. In reality, however, the rotational symmetry is broken owing to various fabrication disorders of the microcavity, giving rise to the mixing of angular momentum. This spoils, to some extent, the ultrahigh Q along with the very large LDOS of the isolated microsphere. On the other hand, we expect that the bisphere cavity is more robust against disorder, because the mixing of angular momentum is already taken into account.

Next, let us consider the emission spectrum of the two-level atom loaded at one of the hot spots $[(x,y,z)=(0.90a,0,0)]$ of the LDOS. From a point of view of experiment, this outer spot is more suitable for loading the atom than the inner spots at $(\pm0.12a,0,0)$. The dipole moment of the atom was taken to be $d=30$ D, which is a typical value of the GaAs quantum dot exciton [42]. The cavity eigenfrequency was chosen such that the cavity at $\omega a/2\pi c=1.2669$ corresponds to 1.5 eV, which is a typical recombination energy in the quantum dot exciton. With this setting, the radius of the spheres is 524 nm. Near the zero detuning $\Omega\simeq\omega_c$, the cQED parameters are evaluated as $g=6.58\times10^{-5}$ eV, $\kappa=1.31\times10^{-5}$ eV, and $\gamma=5.99\times10^{-8}$ eV, yielding the strong coupling between the atom and cavity. Using these parameters, the emission spectrum $S(\omega)$ is plotted as a function of detuning $\Omega-\omega_c$ and frequency. The result is shown in Fig. 3. As is obvious in Fig. 3, an anticrossing is clearly observed between the two "polariton" branches, which come from the mixture of the emission bands of the atom ($\omega=\Omega$) and the cavity ($\omega=\omega_c$). In particular, the double peaks with equal intensity can be found at zero detuning. The vacuum Rabi splitting is given by $\sqrt{4g^2-(\kappa-\gamma/2)^2}=0.131$ meV. As ex-

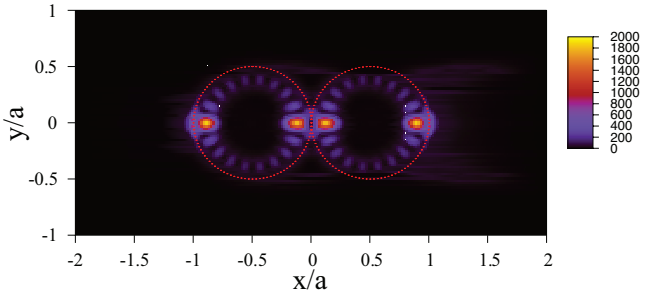

FIG. 2. (Color) The spatial profile of the normalized LDOS $\rho(\mathbf{x};\omega)/\rho_0(\omega)$ in the xy plane. The frequency was taken to be $\omega a/2\pi c=1.2669$, which is the peak frequency of the highest Q in Fig. 1. Solid lines stand for the boundary of the bisphere.

pected, the relative intensity of the band of the atom origin grows as the detuning increases.

Here, we should emphasize that the above results, represented with three cQED parameters g, κ, and γ, are obtained by fitting the LDOS as Eq. (19) around the cavity peak at $\omega a/2\pi c=1.2669$. As is clearly seen in Fig. 1, this peak is at the foot of the broad peak centered around $\omega a/2\pi c=1.2715$. Therefore, a better fitting of the LDOS can be obtained with the sum of two Lorentzian peaks, namely, the cavity peak and the broad peak. The corresponding parameters g_2 and κ_2 of the broad peak satisfies $g_2^2/\kappa_2 \simeq \gamma/2$, while κ_2 is much larger than $\kappa_1(=\kappa)$ of the cavity peak concerned. If we take account of these two peaks, amplitude $b(t)$ of the upper level and the emission spectrum $S(\omega)$ are governed by three roots of $P_3(s)$ ($n=2$ in our case). By numerical calculation we can find that two of the roots, denoted by s_1 and s_2, are very close to $s_\pm$. As a result, $b(t)$ has an additional fast-decaying component proportional to $\exp(ts_3)$ [$\mathrm{Re}(s_3) \ll \mathrm{Re}(s_\pm) \leqslant 0$], whose amplitude is much smaller than the other terms proportional to $\exp(ts_1)$ or $\exp(ts_2)$. Besides, the

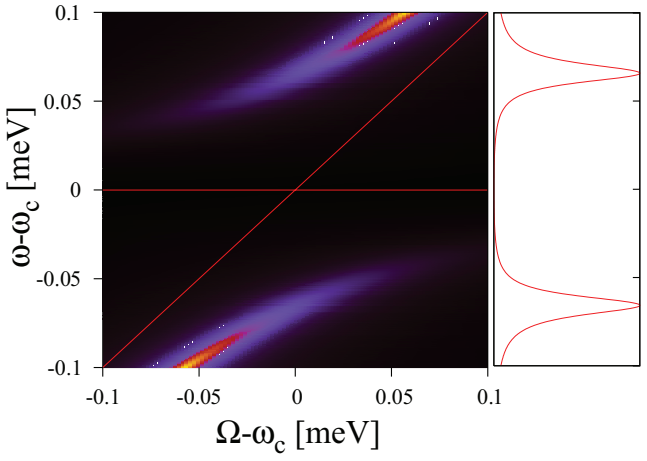

FIG. 3. (Color) Left panel: the contour map of the emission spectrum $S(\omega)$ of the two-level atom whose level spacing Ω is slightly different from the cavity eigenfrequency $\omega_c=1.5$ eV. The cavity line ($\omega=\omega_c$) and the atom line ($\omega=\Omega$) are also shown. The following parameters are used: $g=6.58\times10^{-5}$ eV, $\kappa=1.31\times10^{-5}$ eV, $\gamma=5.99\times10^{-8}$ eV. Right panel: the emission spectrum at the zero detuning $\Omega=\omega_c$.

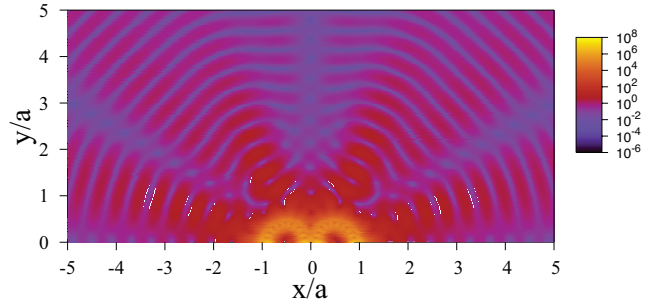

FIG. 4. (Color) The contour map of $f(\mathbf{x};\omega)$ in the xy plane ($z=0$) at a cavity eigenfrequency $\omega a/2\pi c=1.2669$. The two-level atom is placed at $\mathbf{x}=(0.90a,0,0)$. The color map is given in a logarithmic scale.

contribution of the term relevant to s_3 gives an asymmetry in $S(\omega)$ between the double peak of the vacuum Rabi splitting, with respect to peak shape and height. However, the asymmetry is very tiny. Therefore, the approximation of the LDOS given in Eq. (19) is fairly justified.

The above features of the emission spectrum are modified to some extent in the power spectrum of the SE at a local observation point. As we showed in Eq. (11), the power spectrum is a product of two terms, namely, emission spectrum $S(\omega)$ of the two-level atom and the term $f(\mathbf{x};\omega)$ relevant to the photon Green function. Since the photon Green function has a resonance pole at the cavity eigenfrequency concerned, $f(\mathbf{x};\omega)$ becomes very large there irrespective of the observation point $\mathbf{x}$. This implies that even in the case of the strong coupling with zero detuning, the power spectrum can have a peak at $\omega=\omega_c$ aside from the double peaks of the vacuum Rabi splitting. In addition, since $f(\mathbf{x};\omega)$ does not depend on level spacing Ω except for the inessential prefactor proportional to Ω^2, it has the peak irrespective of detuning. Therefore, the power spectrum also exhibits the peak at the cavity eigenfrequency even if the detuning is nonzero. At large nonzero detuning, one of the "polariton" branches is very close in energy to the cavity mode. Thus, it is rather difficult to

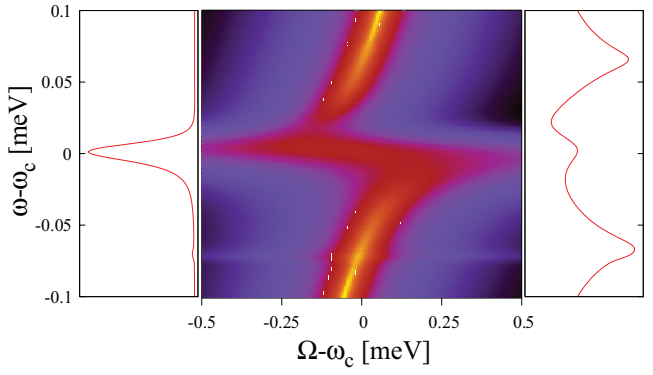

FIG. 5. (Color) Left panel: $f(\mathbf{x};\omega)$ is plotted at $\mathbf{x}=(0,5a,0)$ around $\omega=\omega_c$. Center panel: The contour map of the power spectrum $I(\mathbf{x};\omega)$ at a local observation point [$\mathbf{x}=(0,5a,0)$] is plotted as a function of detuning $\Omega-\omega_c$ and frequency. A similar color map of a logarithmic scale as in Fig. 4 was used. Right panel: The power spectrum at the zero detuning is shown in a logarithmic scale.

distinguish this peak from the "polariton" branches of the cavity origin. Obviously, the relative intensity of the peak depends strongly on the emission spectrum of the two-level atom. Thus, when we argue about the experimental power spectrum of the SE, we should be careful about the identification of the peaks.

Figure 4 shows that the spatial profile of $f(\mathbf{x};\omega)$ in the xy plane at $\omega a/2\pi c=1.2669$. Since $f(\mathbf{x};\omega)$ is related to the dipole radiation field through the photon Green function, it oscillates spatially and thus it is quite sensitive to the spatial coordinate $\mathbf{x}$. This implies that the power spectrum is also sensitive to the observation point. In actual measurement of the power spectrum, we thus have to take account of the spatial extension of the probe, which will be explained with an averaging of $I(\mathbf{x};\omega)$ over an appropriate range of $\mathbf{x}$. In the following, we show the numerical results of the power spectrum in an ideal measurement, which is performed with a pointlike probe.

Let us assume the probe is placed at $\mathbf{x}=(0,5a,0)$. As a function of frequency, $f(\mathbf{x};\omega)$ exhibits a peak at the cavity eigenfrequency. Though the peak shape depends on the position $\mathbf{x}$, it certainly becomes large irrespective of $\mathbf{x}$. Figure 5 shows $f(\mathbf{x};\omega)$ and the power spectrum $I(\mathbf{x};\omega)$ around the cavity eigenfrequency concerned. The left panel shows $f(\mathbf{x};\omega)$ in a linear scale, neglecting the inessential prefactor of Ω^2. The contour map of the power spectrum as a function of detuning and frequency is shown in the center panel. The right panel is the power spectrum at zero detuning. As is obvious in Fig. 5, the peak of $f(\mathbf{x};\omega)$ at $\omega=\omega_c$ strongly affects the power spectrum. In particular, we can see clearly triple peaks in the power spectrum of the SE at zero detuning. This feature forms a striking contrast to the conventional double peaks of the vacuum Rabi splitting in the emission spectrum given in Fig. 3. Moreover, in the power spectrum the peak concerned shifts with detuning in such a way that the two "polariton" branches are connected by the peak. In addition, this peak mixes with the polariton peaks of the cavity origin at large detuning. Because of this mixing, it may be rather difficult to distinguish the polariton peaks from the purely cavity peak in the power spectrum. To be precise, we should note that the center and right panels of Fig. 5 are given in a logarithmic scale. If we plot the power spectrum in a linear scale, the peak at $\omega=\omega_c$ becomes less remarkable compared with the polariton branches.

The condition of having the triple peaks in $I(\mathbf{x};\omega)$ is analyzed as follows. At zero detuning the SE spectrum $S(\omega)$ is given by

$$S(\omega)=\frac{\kappa^2+(\omega-\omega_c)^2}{s_0+s_2(\omega-\omega_c)^2+(\omega-\omega_c)^4}, \tag{59}$$

$$s_0=\left(g^2+\frac{1}{2}\kappa\gamma\right)^2, \quad s_2=\kappa^2+\frac{1}{4}\gamma^2-2g^2, \tag{60}$$

which is a symmetric function with respect to $\omega=\omega_c$. Therefore, $S(\omega)$ at $\omega=\omega_c$ is either peak or dip. The criterion of whether it is peak or dip is not the same as that of whether the system is in the strong coupling or the weak coupling. For instance, there is a certain parameter region of (g,κ,γ) in which $S(\omega)$ exhibits the sharp dip at $\omega=\omega_c$, whereas the system is in the weak coupling. A detailed analysis of the spectral shape of $S(\omega)$ is given in Ref. [43]. On the other hand, $f(\mathbf{x};\omega)$ is approximated as

$$f(\mathbf{x};\omega)=\frac{\sum_{k=0}^{4} f_k(\omega-\omega_c)^k}{[(\omega-\omega_c)^2+\kappa^2]^2}, \tag{61}$$

by employing an asymmetric Fano profile for $\rho_{ij}(\mathbf{x},\mathbf{x}_d;\omega)/\rho_0(\omega)$. To determine f_k $(k=0,\ldots,4)$ a precise calculation of the photon Green function is needed. If they are available, the condition of having the cavity peak in $I(\mathbf{x};\omega)$ is estimated as

$$\frac{f_2}{f_0}-\frac{s_2}{s_0}<\frac{1}{\kappa^2}, \tag{62}$$

though the peak is slightly shifted owing to the presence of the f_1 term. We confirmed this inequality holds in our system. To the best of our knowledge, no one has reported on the triple peaks around the zero detuning in the strong-coupling regime of the power spectrum of the SE. This may be related to the oscillating behavior of $f(\mathbf{x};\omega)$ and to the smallness of the cavity peak in comparison to the polariton peaks. We expect that this peak will be observed with a pointlike probe of high sensitivity.

VI. SUMMARY

In summary, we have formulated a theory of the SE dynamics of a two-level atom embedded in a general structured reservoir. The photon Green function plays a crucial role there. In the case of the reservoir that includes a cavity mode, we have addressed the relation between our approach and the conventional one of cQED. In particular, a simple recipe to determine the cQED parameters was given. Then, we have developed a method to calculate the photon Green function in a cluster of nonoverlapping microspheres as a structured reservoir. A detailed analysis was made for a bisphere system, which has a sequence of cavity modes with high quality factor with small modal volume. By using a high Q cavity mode, we have demonstrated the strong coupling between the atom and cavity. The precise calculation of the photon Green function in the system enables us to evaluate the power spectrum at a given observation point. The spectrum is shown to be the product of the emission spectrum of the two-level atom and the term coming from the photon Green function. Owing to the resonance pole of the photon Green function at the cavity eigenfrequency, the power spectrum at zero detuning does not simply exhibit the conventional double peaks of the vacuum Rabi splitting in the strong-coupling regime. Instead, the spectrum can exhibit a small peak at the cavity eigenfrequency in addition to the double peaks. The triple peaks of the power spectrum may be observed with a pointlike probe with high sensitivity.

Finally, we should stress again that the results obtained in this paper are quite general and are applicable to other types

of cavity, not being limited in the bisphere cavity concerned. In particular, the triple peaks of the power spectrum of the SE in the strong-coupling regime will appear also in (isolated) microsphere cavity, microdisk cavity, photonic crystal cavity, and so on. The bisphere cavity was chosen solely because it is a simple, but nontrivial structured reservoir, having a unique spatial profile of the LDOS. A similar analysis in more realistic cavities will be important for various applications in optoelectronics and quantum information processing.

ACKNOWLEDGMENTS

The authors would like to thank T. Kuroda of NIMS for valuable discussions. This work was supported by a Grant-in-Aid for Scientific Research from the Ministry of Education, Science, Sports and Culture of Japan.

[1] K. J. Vahala, Nature (London) **424**, 839 (2003).
[2] Y. Akahane, T. Asano, B. S. Song, and S. Noda, Nature (London) **425**, 944 (2003).
[3] B. S. Song, S. Noda, T. Asano, and Y. Akahane, Nat. Mater. **4**, 207 (2005).
[4] L. Collot, V. Lefevreseguin, M. Brune, J. M. Raimond, and S. Haroche, Europhys. Lett. **23**, 327 (1993).
[5] H. Miyazaki and Y. Jimba, Phys. Rev. B **62**, 7976 (2000).
[6] T. Mukaiyama, K. Takeda, H. Miyazaki, Y. Jimba, and M. Kuwata-Gonokami, Phys. Rev. Lett. **82**, 4623 (1999).
[7] Y. Hara, T. Mukaiyama, K. Takeda, and M. Kuwata-Gonokami, Phys. Rev. Lett. **94**, 203905 (2005).
[8] P. Lambropoulos, G. M. Nikolopoulos, T. R. Nielsen, and S. Bay, Rep. Prog. Phys. **63**, 455 (2000).
[9] *Cavity Quantum Electrodynamics*, edited by P. Berman, (Academic, San Diego, 1994).
[10] E. Purcell, Phys. Rev. **69**, 681 (1946).
[11] J. P. Reithmaier, G. Sęk, A. Löffler, C. Hofmann, S. Kuhn, S. Reitzenstein, L. V. Keldysh, V. D. Kulakovskii, T. L. Reinecke, and A. Forchel, Nature (London) **432**, 197 (2004).
[12] T. Yoshie, A. Scherer, J. Hendrickson, G. Khitrova, H. M. Gibbs, G. Rupper, C. Ell, O. B. Shchekin, and D. G. Deppe, Nature (London) **432**, 200 (2004).
[13] E. Peter, P. Senellart, D. Martrou, A. Lemaitre, J. Hours, J. M. Gérard, and J. Bloch, Phys. Rev. Lett. **95**, 067401 (2005).
[14] H. J. Carmichael, R. J. Brecha, M. G. Raizen, H. J. Kimble, and P. R. Rice, Phys. Rev. A **40**, 5516 (1989).
[15] H. Chew, J. Chem. Phys. **87**, 1355 (1987).
[16] H. Chew, Phys. Rev. A **38**, 3410 (1988).
[17] V. V. Klimov, M. Ducloy, and V. S. Letokhov, Phys. Rev. A **59**, 2996 (1999).
[18] J. Ushida, T. Ohta, and K. Cho, J. Phys. Soc. Jpn. **68**, 2439 (1999).
[19] D. W. Vernooy, A. Furusawa, N. P. Georgiades, V. S. Ilchenko, and H. J. Kimble, Phys. Rev. A **57**, R2293 (1998).
[20] X. D. Fan, P. Palinginis, S. Lacey, H. L. Wang, and M. C. Lonergan, Opt. Lett. **25**, 1600 (2000).
[21] V. S. Ilchenko, M. L. Gorodetsky, X. S. Yao, and L. Maleki, Opt. Lett. **26**, 256 (2001).
[22] A. Kiraz, P. Michler, C. Becher, B. Gayral, A. Īmamoglu, L. D. Zhang, E. Hu, W. V. Schoenfeld, and P. M. Petroff, Appl. Phys. Lett. **78**, 3932 (2001).
[23] J. R. Buck and H. J. Kimble, Phys. Rev. A **67**, 033806 (2003).
[24] T. Baba and D. Sano, IEEE J. Sel. Top. Quantum Electron. **9**, 1340 (2003).
[25] S. M. Spillane, T. J. Kippenberg, K. J. Vahala, K. W. Goh, E. Wilcut, and H. J. Kimble, Phys. Rev. A **71**, 013817 (2005).
[26] L. A. Blanco and F. J. García de Abajo, Phys. Rev. B **69**, 205414 (2004).
[27] R. Sprik, B. A. VanTiggelen, and A. Lagendijk, Europhys. Lett. **35**, 265 (1996).
[28] S. Hughes, Opt. Lett. **30**, 1393 (2005).
[29] N. Vats, S. John, and K. Busch, Phys. Rev. A **65**, 043808 (2002).
[30] M. O. Scully and M. S. Zubairy, *Quantum Optics* (Cambridge University Press, Cambridge, 1997).
[31] A. O. Caldeira and A. J. Leggett, Phys. Rev. Lett. **46**, 211 (1981).
[32] H. M. Lai, P. T. Leung, and K. Young, Phys. Rev. A **37**, 1597 (1988).
[33] B. J. Dalton, S. M. Barnett, and B. M. Garraway, Phys. Rev. A **64**, 053813 (2001).
[34] M. Lewenstein, J. Zakrzewski, and T. W. Mossberg, Phys. Rev. A **38**, 808 (1988).
[35] L. C. Andreani, G. Panzarini, and J. M. Gérard, Phys. Rev. B **60**, 13276 (1999).
[36] P. Stehle, Phys. Rev. A **2**, 102 (1970).
[37] A. Taflove and S. C. Hagness, *Computational Electrodynamics: The Finite-Difference Time-Domain Method* (Artech House, Boston, 2005).
[38] *Photonic Crystals*, edited by K. Inoue and K. Ohtaka, (Springer, Berlin, 2004), p. 58.
[39] M. Inoue and K. Ohtaka, J. Phys. Soc. Jpn. **52**, 3853 (1983).
[40] K. Ohtaka, Phys. Rev. B **19**, 5057 (1979).
[41] F. J. García de Abajo, Phys. Rev. B **60**, 6086 (1999).
[42] T. Kuroda, K. Kuroda, K. Sakoda, K. Watanabe, N. Koguchi, and G. Kido, Proc. SPIE **6115**, 61151L (2006).
[43] J. Inoue, T. Ochiai, and K. Sakoda, J. Phys. Soc. Jpn. **75**, 094720 (2006).